# CMIP6 models underestimate the Holton-Tan effect

**Dillon Elsbury[1], Yannick Peings[1], and Gudrun Magnusdottir[1]**

[1]University of California, Irvine, Department of Earth System Science

Corresponding author: Dillon Elsbury (delsbury@uci.edu): orcid: 0000-0002-3730-9226

**Key Points:**

- The CMIP6 models underestimate the weakening of the polar vortex expected when QBO easterlies exist in the tropical lower stratosphere
- Potential vorticity (PV) maps reveal that pooling of PV over mid-latitude Asia is important for coupling the QBO with the polar vortex
- The models underestimate the teleconnection because the 10 hPa QBO westerlies are too weak and too narrow

## Abstract

The teleconnection between the Quasi-Biennial Oscillation (QBO) and the Arctic polar vortex is investigated using Coupled Model Intercomparison Project phase 6 (CMIP6) models. We use 14 CMIP6 models, reanalysis, three experiments with prescribed QBOs, one of which has no free polar stratospheric variability, and branched runs in which a QBO is imposed in runs previously devoid of a QBO. Each CMIP6 model underestimates the Holton-Tan effect (HTE), the weakening of the polar vortex with QBO easterlies in the lower stratosphere. To establish why, 850 Kelvin potential vorticity (PV) maps are used to study zonal asymmetries in the teleconnection. The QBO initiates the HTE by promoting equatorward (poleward) intrusion of high (low) PV over mid-latitude Asia (60°E-120°E). The presence of the PV intrusion in a model response is highly correlated with polar cap warming and the HTE. Models with stronger 10 hPa QBO amplitudes generally include the PV intrusion.


## Plain Language Summary

In the tropics at altitudes between two and three times as high as commercial airplanes cruise, the winds alternate between blowing to the east for about a year before switching direction and blowing to the west for the next year. This pattern of winds is called the Quasi-Biennial Oscillation (QBO). Despite being high up in the tropical atmosphere, the QBO affects the global circulation in ways that ultimatey influence regional weather. One example of this occurs during winter, when the QBO changes the strength of the jet-stream. Althouch scientists have known about this phenomenon for

over 40 years, this long-distance relationship is complicated. Models of the coupled land, ocean, atmosphere system have steadily improved at representing the QBO. These models also represent the QBO's relationship with the jet-stream, but each model does it differently. We evaluate how the models perform in this study. The difference between models that represent the QBO-jet-stream relationship well and models that do not teaches us more about the relationship. We learn here that the QBO begins communicating with the jet by changing the atmospheric circulation 30 kilometers above Asia, nearly over the Tibetan Plateau. This phenomenon is best represented by models that have stronger QBOs.

## 1 Introduction

The Quasi-Biennial Oscillation (QBO) influences the global circulation through a suite of teleconnections (Gray et al. 2018). It modulates tropical convection (Son et al. 2017), upper tropospheric mid-latitude flow (Wang et al. 2018; Hitchman et al. 2021), and polar stratospheric flow in the southern (Yamashita et al. 2018) and northern hemispheres (Holton and Tan 1980; Lu et al. 2020). Each teleconnection is sensitive to the QBO's structure, its meridional extent (Hansen et al. 2013), the configuration of its easterly and westerly jets (Garfinkel et al. 2012; Gray et al. 2018), its vertical extent (Andrews et al. 2019), and how deep it reaches into the lower stratosphere (Collimore et al. 2003). Now with the Coupled Model Intercomparison Project 6 (CMIP6) models spontaneously generating the QBO, there is variability in how the models represent its structure (Richter et al. 2020). This suggests that there is variability in how the models represent the QBO teleconnections (Rao et al. 2020a,b). This study focuses on one of these

teleconnections, the boreal winter polar stratospheric response to the QBO, the Holton-Tan effect (HTE, Holton and Tan 1980). We have two goals: (1) better understand why the CMIP6 models underestimate the HTE (Fig. 1) while (2) also learning how the middle stratospheric, 850 Kelvin, branch of the teleconnection varies over longitude.

When QBO westerlies are in the middle stratosphere (10 hPa) and QBO easterlies in the lower stratosphere (50 hPa), the polar vortex is weaker than in climatology. This configuration of the QBO, denoted $QBO_{E50}$, influences where planetary wave breaking occurs in the stratosphere (Hitchman and Husesmann 2009; Lu et al. 2020). QBO easterlies concentrate planetary waves and their breaking into the northern hemisphere (Holton and Tan 1980; Lu et al. 2020). The QBO induced mean meridional circulation (QBO-MMC) is also important for this teleconnection.

The QBO-MMC acts as a residual mean meridional circulation that maintains the dynamically forced temperature response to the QBO against radiative relaxation (Plumb and Bell 1982; Pahlavan et al. 2021; Hitchman et al. 2021). Westerly (easterly) QBO shear coincides with tropical warming (cooling), which is generated by adiabatic descent (ascent). At subtropical to mid-latitudes, the QBO-MMC induces vertical motion in the opposite direction of that in the tropics, yielding opposite temperature responses (Fig. 1q). The QBO-MMC changes the mid-latitude middle stratospheric mean flow geometry, forcing more poleward refraction of planetary waves (Garfinkel et al. 2012; Lu et al. 2014), which would otherwise propagate equatorward. This weakens the polar vortex.

It is not clear how this process varies over longitude. We hypothesize that it does as the QBO demonstrates zonally asymmetric teleconnections elsewhere. It has unique impacts on the North Pacific and North Atlantic jets (Wang et al. 2018). Further, we find that the QBO preferentially communicates with the mid-latitude North Pacific lower stratosphere by inducing more planetary wave absorption there relative to other longitudes (Elsbury et al. 2021). A more speculative hypothesis is that the QBO's zonally asymmetric structure (Hamilton et al. 2004; Hitchman and Huesmann 2009; Tegtmeier et al. 2020) predisposes it to have zonally asymmetric impacts on the extratropical circulation.

## 2 Methods

The HTE is analyzed over the 1850-2014 period using the same historical CMIP6 models used by Richter et al. (2020) to facilitate comparison between the extratropical responses (this study) and the QBO qualities in each model (their study). The CMIP6 responses to the QBO are compared to 1979-2019 ERA5 reanalysis (Hersbach et al. 2020).

Four experiments with the specified chemistry version of the Whole Atmosphere Community Climate Model (SC-WACCM4, Smith et al. 2014) use a prescribed QBO and are therefore useful for comparing with the CMIP6 models. The model domain is the surface up to 145 kilometers over 66 vertical levels with horizontal resolution of 1.9° latitude, 2.5° longitude. To simulate the QBO, the tropical stratospheric winds from 86

hPa-4 hPa and 22°S-22°N are relaxed toward a climatological 28-month QBO cycle derived from radiosondes (Hansen et al. 2013). The first of the experiments, referred to as PAMIP-WCSC, is a 1500-year simulation with a repeating annual cycle of sea surface temperature (SST) corresponding to present-day climate and a suite of different Arctic sea ice forcings (we neglect a potential influence of Arctic sea ice conditions on the QBO teleconnections). The second experiment, AMIP-WCSC, is a 370-year dataset made up of 10 ensemble members, run from 1978 to 2016, forced by the observed chronology of SST and sea ice variability. The third experiment, CPS-WCSC, is a 300-year simulation forced in the same way as PAMIP-WCSC except the polar stratospheric variability poleward of 60°N is relaxed toward a climatological polar stratospheric state allowing us to diagnose the influence of the QBO on the atmosphere in the absence of a polar stratospheric response to the QBO. The fourth experiment allows us to diagnose the transient atmospheric response to imposing the QBO. A 100-year control simulation devoid of the prescribed QBO is run and restarts are saved for each November 1$^{st}$. We branch from November 1$^{st}$ and then impose the $QBO_{E50}$ profile. The QBO propagates downward and the runs last until January 31$^{st}$. More details on PAMIP-WCSC, CPS-WCSC, and the transient runs are given in Elsbury et al. (2021).

Throughout the manuscript, anomalies are calculated as deviations from the seasonal cycle. These anomalies are then subsampled by QBO phase. The $QBO_{E50}$ index can be defined using westerlies at 10 hPa or easterlies at 50 hPa. Both yield similar results. However, the latter captures non-QBO variability for some models. Therefore, the $QBO_{E50}$ index is defined as the December-January (DJ) time averaged, longitudinally

128 averaged, and latitudinally averaged winds between 5°S and 5°N at 10 hPa that exceed
129 2.5 m/s. Further, similar results are obtained using the phase angle 30 hPa QBO index
130 of Huang et al. (2012). This index allows for more control in picking the vertical structure
131 of the QBO we are interested in, e.g., easterlies at 50 hPa (Fig. S1). Results are
132 consistent for all three QBO indices. Here we present results using the $QBO_{E50}$ index
133 and have phase angle duplicates of Fig. 1 and 4 in supplementary (Fig.S2, Fig. S3).
134

135 **3 Results**

136 **3.1 Zonal mean zonal wind**

137 Figure 1 shows zonal mean zonal wind anomalies for all 18 datasets. The models both
138 overestimate (1b, g, j, o, p) and underestimate (all others) the peak 10 hPa QBO
139 westerlies relative to ERA5 (shown by Richter et al. 2020). The QBO westerlies extend
140 upward and poleward between 20°N-40°N in ERA5, but they are confined equatorward
141 in CMIP6 models. Each CMIP6 QBO is narrow relative to ERA5 (10 hPa QBO widths
142 printed above plots).
143

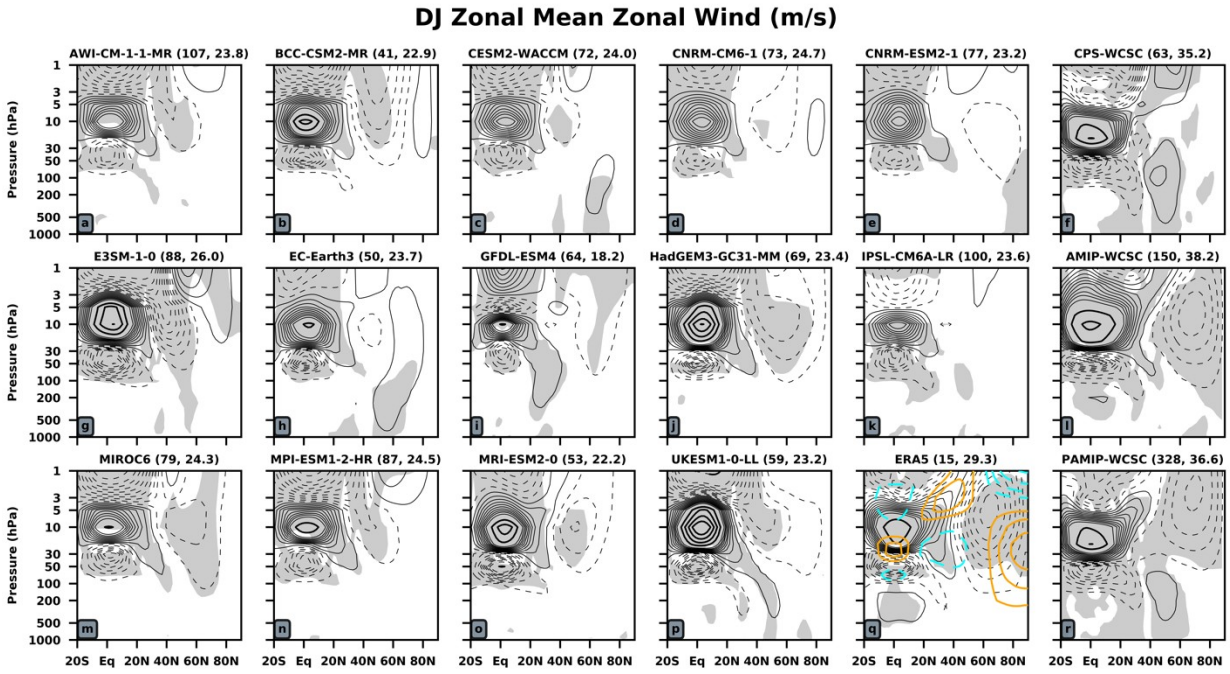


Figure 1: DJ zonal mean zonal wind anomalies. Thin contours show anomalies between +/- 8.5 m/s with intervals of +/- 1m/s. Thick contours correspond to +10, 15, 20 … m/s. Gray shading denotes statistical significance, p-values < 0.05 via a student's t-test, when comparing $QBO_{E50}$ anomalies to all other anomalies. To the right of model titles is the number of DJ periods averaged together to make each composite and the 10 hPa latitudinal width of the QBO. Widths are calculated by applying the "half-maximum" method of Richter et al. (2020) and Bushell et al. (2020) to the anomalous 10 hPa response from each plot. Warm (cool) temperature anomalies are shown on Flg. 1q with +/- 1 K contours.

The 50 hPa peak QBO easterlies match ERA5 in four cases (1g, j, o, p) and are underestimated otherwise. Each unique QBO coincides with unique tropical stratospheric temperature perturbations (not shown), which the QBO-MMC must maintain against radiative relaxation. Therefore, the QBO-MMC differs in each model. Prescribing the QBO ensures that it has sufficient lower stratospheric amplitude. The QBO, in the absence of a HTE, pushes the tropospheric jet poleward (CPS, Fig. 1f). This is moderated by an equatorward jet shift in AMIP and PAMIP (Fig. 1l,r) due to a warm polar stratosphere caused by the HTE (Elsbury et al. 2021, Fig. 6). These

experiments with prescribed QBOs show that when a realistic QBO exists in the model, teleconnections more closely resemble observations, notably the HTE.

While some models simulate a weakening of the polar stratospheric winds (BCC-CSM2-MR, HadGEM3-GC31-MM, MIROC6, UKESM1-0-LL), each model underestimates the HTE relative to ERA5 (Fig. 1q) and the prescribed QBO runs (Fig 1l, r). AWI-CM-1-1-MR, E3SM-1-0, MPI-ESM1-2-HR, and MRI-ESM2-0 each have extratropical easterly anomalies, but they are not at polar latitudes. Underestimation of the HTE occurs with all three QBO indices (Fig. S2). This should hinder stratospheric interaction with the tropospheric jet.

### 3.2 Zonally asymmetric middle stratospheric teleconnection

Before assessing the representation of the middle stratospheric HTE, we need to establish what this teleconnection looks like in a zonally asymmetric sense. Figure 2 shows potential vorticity (PV) on the 850 Kelvin isentropic surface (approximately 10hPa) associated with $QBO_{E50}$ in ERA5. The standard deviation of the field shows that PV varies between 20 and 50 PVU from 30°N to 30°S with larger variability in the North Atlantic mid-latitudes than in the North Pacific (Fig. 2b). The largest variations occur at polar latitudes, especially over the North Pacific.

Relative to the standard deviation, the $QBO_{E50}$ dominates the tropical and subtropical 850 K PV variability (Fig. 2a). At polar latitudes, the polar vortex is most disturbed over the North Atlantic where low PV anomalies peak at -60 PVU, about 50% of the |

183 standard deviation| there. Fig. 2a mirrors the DJ 850 K first empirical orthogonal
184 function, which accounts for 36% of the variance (Fig. S4).
185

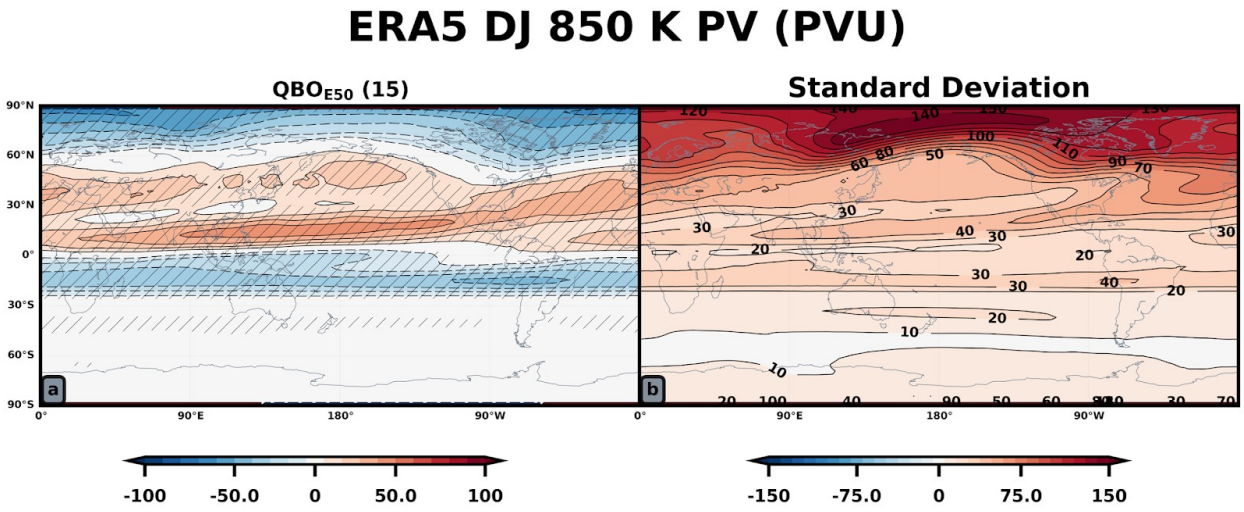


186

187 Figure 2: ERA5 DJ 850 Kelvin PV anomalies. Anomalies are deviations from the seasonal cycle for QBO$_{E50}$ indices. Hatching
188 denotes statistical significance, p-values < 0.05 via a student' t-test, when comparing QBO$_{E50}$ anomalies to all other anomalies. The
189 contour interval in line and shading for all panels is +/- 10 PVU. Fifteen DJ seasons are used to make the composite (a). Panel (b)
190 shows the standard deviation of the field with contour intervals 10, 20, 30… PVU.
191

192 Two bands of anomalous PV span the tropics, negative in the southern hemisphere,
193 positive in the northern hemisphere (Fig. 2a). This is the signature of the QBO-MMC.
194 Shown by Hitchman and Huesmann (2009), the QBO-MMC converges toward the base
195 of the QBO westerlies, "pinching" together the PV contours: high PV from the northern
196 hemisphere and low PV from the southern hemisphere are concentrated nearer the
197 tropics. The negative PV anomaly in the southern hemisphere shows some zonal
198 asymmetry while the northern hemisphere positive PV band shows strong variation over
199 longitude.
200

Since internal variability may convolute these PV results, we look for these signatures in dedicated perturbation experiments. Figure 3 shows the evolution of the PV field once a downward propagating $QBO_{E50}$ profile is imposed in the control simulation devoid of a QBO. Anomalies are calculated as the difference between the transient runs and control runs from which the transient simulations are branched.

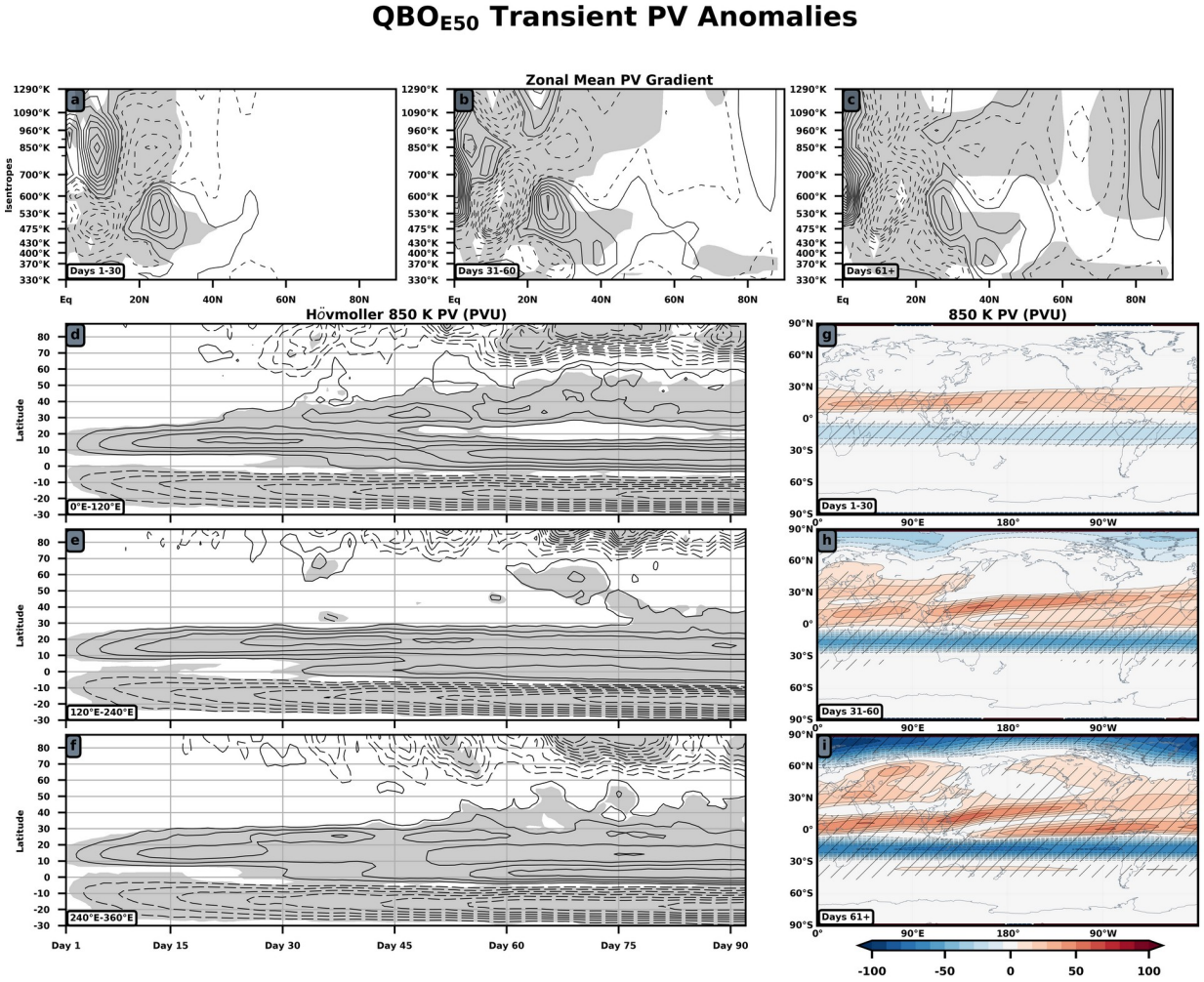


Figure 3: Anomalies after imposing a $QBO_{E50}$ profile in the transient runs. (a-c): Zonal mean meridional PV gradient for successive 30-day periods after branching: dashed-negative (solid-positive) contours begin at negative (positive) $1x10^{-7}$ $K \cdot m \cdot kg^{-1} \cdot s^{-1}$ and decrease (increase) by negative (positive) $5x10^{-7}$ $K \cdot m \cdot kg^{-1} \cdot s^{-1}$ intervals. The responses at each isentrope are multiplied by $(\theta/350)^{9/2}$ to account for logarithmic change in PV with height. (d-f): Latitude-time Hövmollers of 850 Kelvin PV (+/- 10 PVU) averaged over 0°E-120°E (d), 120°E-240°E (e), and (f) 240°E-360°E. Gray shading denotes statistical significance in (a-f), p-values < 0.05 via a

213 student's t-test, when comparing $QBO_{E50}$ and control responses. (g-h) Maps of 850 K PV (+/- 10 PVU) anomalies with hatching
214 denoting statistical significance.
215

216 Figs. 3a-c shows change in the meridional gradient of the zonal mean PV, $P_\varphi$, once the
217 $QBO_{E50}$ is imposed. Negative anomalies mean that the PV gradient is decreased and
218 linear wave propagation into the region is less likely while the opposite holds true for
219 regions with positive anomalies. During days 1-30, QBOW is located around 850 K and
220 QBOE around 530 K. Planetary waves may propagate through the 850 K westerlies, but
221 not the 530 K easterlies (Fig. 3a). $P_\varphi$ weakens in the middle stratosphere between 30°N-
222 50°N during days 31-60 indicating reduced likelihood for equatorward propagation (Fig.
223 3b). Beyond day 61, the polar stratospheric gradient weakens and this signal
224 propagates downward (Fig. 3c). How does the spatiotemporal evolution of PV look on a
225 horizontal surface, if we do not take a zonal average?
226

227 During the first 30 days at 850 K, the QBO-MMC spins up (Figs. 3g-i). The two
228 anomalous PV bands indicate equatorward motion of the QBO-MMC from both
229 hemispheres and the signal is almost zonally symmetric with more pooling of high PV
230 near Asia (Fig. 3g). During the next 30 days, the positive PV anomalies become more
231 zonally asymmetric, tilting out of the tropics toward the east (Fig. 3h). The evolution of
232 the anomalous negative PV gradient poleward seen in the zonal mean occurs over
233 Eurasia between 30°N and 50°N (Fig. 3h). Pooling of high PV over these continents is
234 consistent with dilution of high PV over the pole during the last 32 days of the
235 simulations (Fig. 3i).
236

Latitude-time Hövmollers make clear the importance of the Eurasia sector for coupling the QBO with the polar vortex (Figs. 3d-f). Equatorward (poleward) intrusion of high (low) PV occurs between 0°E-120°E during days 30-45 (Fig. 3d). Importantly, this anomalous flattening of the PV gradient (Fig. 3d) leads the other sectors (Fig. 3e-f). Fig. 3 suggests that the HTE begins in the middle stratosphere (Fig. 3a-c), particularly over Eurasia (Fig. 3d,h).

While the PV intrusion is broadly located over Africa, Europe, and Asia, subsequent results will show that the PV response over mid-latitude Asia is most important for the HTE. Therefore, we hereafter refer to this regional PV response as the "PV intrusion" or "Asia $P_{\varphi}$."

### 3.3 Middle stratosphere in the CMIP6 models

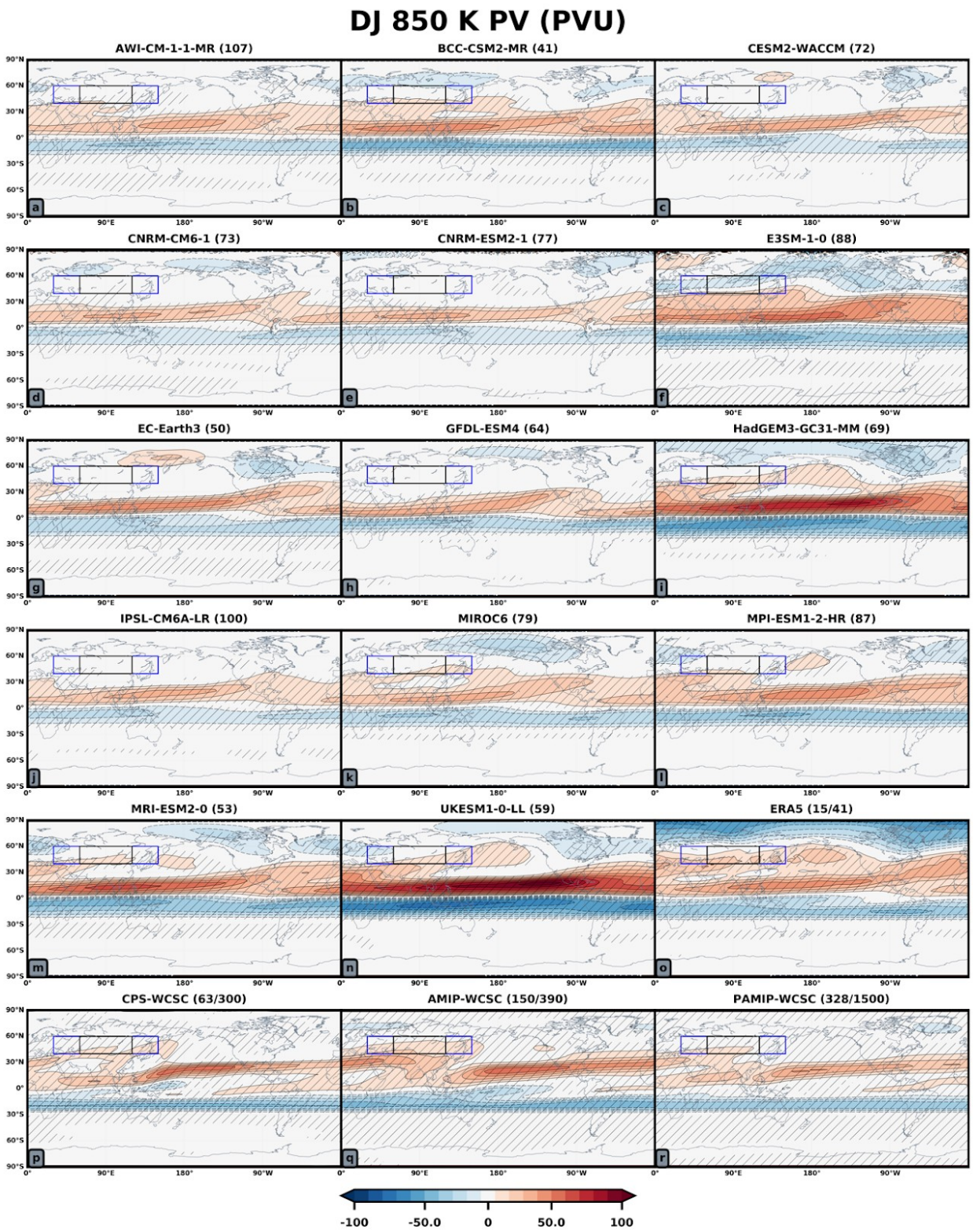


Figure 4: DJ 850 K PV anomalies for the 18 datasets. Contour intervals are +/- 10 m/s. Hatching denotes statistical significance, p-values < 0.05 via a student's t-test, when comparing $QBO_{E50}$ anomalies to all other anomalies. Black and blue rectangles denote where the anomalous $_{P}$ is highly correlated with polar cap warming (Table S1).

Figure 4 shows 850 K PV anomalies for each model. From Fig. 1, the models that exhibit extratropical easterlies at polar latitudes (BCC-CSM2-MR, HadGEM3-GC31-MM, MIROC6, UKESM1-0-LL) or mid-latitudes (AWI-CM-1-1-MR, E3SM-1-0, MPI-ESM1-2-HR, MRI-ESM2-0) exhibit intrusion of high PV over mid-latitude Asia. Models with weaker HTEs (CESM2-WACCM, CNRM-CM6-1, CNRM-ESM2-1, EC-Earth3, GFDL-ESM4, IPSL-CM6A-LR) exhibit no pooling of PV over Asia. The CMIP6 PV intrusions are equatorward of the intrusions in ERA5 or SC-WACCM4, suggesting why the CMIP6 extratropical easterly anomalies are ubiquitously equatorward of the polar stratosphere in Fig. 1. Note that every dataset's QBO is zonally asymmetric with stronger flow around Indonesia or the Indian Ocean, which may explain the location of the PV intrusion (Fig. S5).

Enhanced PV over Asia indicates anomalous cyclonic flow there. Stronger westerlies on its equatorward flank should strengthen $P_{\varphi}$ and reduce wave breaking. Stronger easterlies on its poleward flank should weaken $P_{\varphi}$ and reduce wave propagation. Indeed, studies using reanalysis (Fig. 3b of Lu et al. 2014) and model experiments (Garfinkel et al. 2012) show that $QBO_{E50}$ suppresses climatological equatorward planetary wave propagation at 850 K between 30°N and 50°N in favor of anomalous poleward propagation. These PV results corroborate those studies and we add and emphasize that this process occurs over Asia.

Fig. 5 suggests that the PV intrusion is associated with the HTE. It establishes the relation between the anomalous polar cap temperatures at 10 hPa and $P_\varphi$ averaged between 40°N and 60°N over various 60° longitude windows (Table S1). Various 60° longitude windows are used to see over what longitudes $P_\varphi$ is most strongly associated with the polar cap temperature anomalies. Correlations exceed 0.7 from 30°E-150°E and peak at 0.82 from 60°E-120°E (Table S1). This is where the PV intrusion is located (enclosed by rectangles in Fig. 4). Fig. 5a depicts the relationship between Asia $P_\varphi$ and polar cap temperatures. The more negative Asia $P_\varphi$ is, the warmer the polar cap is (Fig. 5a).

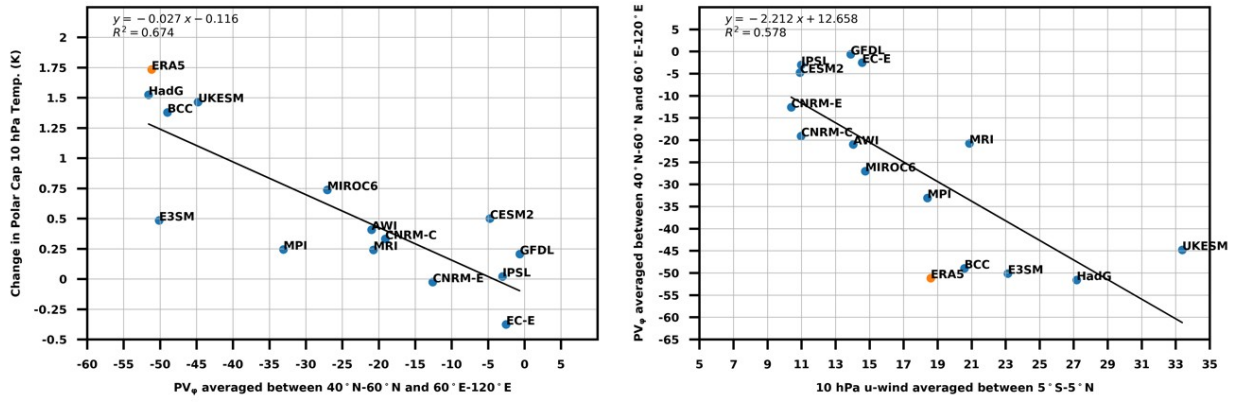


Figure 5: Left: The anomalous meridional PV gradient ($_\varphi$) over Asia is compared to the anomalous 10 hPa polar cap (60°N+) temperature. $_\varphi$ is not divided by the radius of Earth when calculating it. Right: The anomalous 10 hPa QBO, longitudinally averaged and cosine weighted latitudinally averaged zonal winds between 5°S-5°N, of Figure 1 are compared to $_\varphi$ over Asia.

Asia $P_\varphi$ is a direct response to the QBO – it does not result from the HTE. Indeed, the PV intrusion exists in the CPS 850 K response, which reveals the impact of the QBO in the absence of a polar stratospheric response (Fig. 4r). Furthermore, imposing the QBO in the transient simulations promoted the PV intrusion (Fig. 3). Regression between the 10 hPa QBO westerly velocity and Asia $P_\varphi$ shows that stronger QBO winds equate to

295 more negative Asia $P_\varphi$ (Fig. 5b). Citing the strong relationship between Asia $P_\varphi$ and
296 polar cap temperatures, underestimation of the 10 hPa QBO amplitudes is *partly*
297 suppressing the HTE.
298

299 **4 Discussion**

300 **4.1 Importance of the QBO-MMC**

301 Stronger QBOs have larger effects on the extratropical circulation. Of the 14 CMIP6
302 models, the eight with strongest 10 hPa QBO westerlies are BCC-CSM2-MR,
303 HadGEM3-GC31-MM, MIROC6, UKESM1-0-LL, AWI-CM-1-1-MR, E3SM-1-0, MPI-
304 ESM1-2-HR, and MRI-ESM2-0 (Fig. 5b, compare with Fig. 2b of Richter et al. 2020).
305 The first four models feature some weakening of the polar vortex while the latter four
306 exhibit anomalous easterlies equatorward of the polar vortex. The models with the
307 weakest 10 hPa QBO westerlies exhibit much weaker easterlies everywhere in the
308 stratosphere (Fig. 1c, d, e, h, i, k).
309

310 Our Figs. 4 and 5b show that models with stronger 10 hPa QBO amplitudes feature
311 stronger PV intrusions over Asia. Garfinkel and Hartmann (2011, Fig. 6) show that
312 stronger QBOs have stronger QBO-MMCs, which have larger effects on the
313 extratropical circulation. A speculation then is that the PV intrusion may be the
314 extratropical signature of the QBO-MMC. By underestimating this feature, which
315 confines planetary waves to higher latitudes (Lu et al. 2014), the models underestimate
316 the HTE.

317

318 **4.2 Limitations of our argument**

319 Underestimating the 10 hPa QBO amplitudes is not the only factor hindering the HTEs.
320 For instance, HadGEM3-GC31-MM and UKESM1-0-LL both overestimate the 10 hPa
321 QBO winds and still underestimate the weakening of the polar vortex relative to ERA5
322 (Fig. 1j,p).

323

324 Figure 1 shows that the QBOs are too narrow. We calculate the latitudinal extents of the
325 QBOs at 10 hPa using the "half-maximum" method of Richter et al. (2020) and Bushell
326 et al. (2020); see the model titles in Fig. 1. Regression between these extents and Asia
327 $P_{\varphi}$ shows little correlation (Fig. S6). Regardless, Hansen et al. (2013) have already
328 shown that narrow QBOs coincide with a reduced HTE.

329

330 **5 Conclusions**

331 The HTE is analyzed in the CMIP6 historical simulations studied by Richter et al. 2020.
332 The CMIP6 models consistently underestimate the amplitude of the HTE during
333 December and January relative to ERA5. This conclusion is robust to three different
334 QBO indices.

335

336 The underestimation of the HTE coincides with underestimation of the 10 hPa QBO
337 amplitudes. The desired impact that the models are not representing is the intrusion of
338 high PV anomalies over Asia. This signal is highly anticorrelated with polar stratospheric
339 warming taking place during $QBO_{E50}$. The transient simulations in which the QBO is

imposed in a live running atmosphere devoid of a QBO, and CPS, which includes no polar stratospheric variability, both suggest that the QBO promotes the intrusion of high PV air over Asia *by itself*. Further, the presence of this signal in the CMIP6 models that simulate HTE, the 1500-year SC-WACCM4 simulation set, and ERA5 suggest this is an important feature for the teleconnection in nature.

Why does the PV intrusion occur over Asia? The QBO has a stronger amplitude over that sector (Fig. S5), but other factors may play a role too. For instance, orographic gravity wave drag over the Tibetan Plateau has a nonnegligible influence on the stratospheric mean flow (Xu et al. 2017). This will have to be investigated in future work.

## Acknowledgments, Samples, and Data

High performance computing support is generously provided by the National Center for Atmospheric Research, sponsored by the National Science Foundation (NSF). doi:10.5065/D6RX99HX. CMIP6 data is archived very nicely and provided by the Earth System Grid Federation (https://esgf-node.llnl.gov/search/cmip6/). Thank you to various modeling agencies who have run the simulations, processed the data, and made it publicly available. ERA5 reanalysis may be accessed with Copernicus (https://cds.climate.copernicus.eu/cdsapp#!/dataset/10.24381/cds.bd0915c6?tab=overview). doi:10.24381/cds.bd0915c6. This study is supported by the NSF, Division of Graduate Education, DGE-1839285, and the Department of Energy, Office of Biological Environment Research, DE-SC0019407. Reviewers, we will add our CPS, AMIP, PAMIP, and transient simulation data to Zenodo once we go through the review

process. You can only submit data there once as submitting your data coincides with receiving a unique doi, which is meant to go in the acknowledgements.

## References

Andrews, M. B., Knight, J. R., Scaife, A. A., Lu, Y., Wu, T., Gray, L. J., & Schenzinger, V. (2019). Observed and simulated teleconnections between the stratospheric quasi‐biennial oscillation and Northern Hemisphere winter atmospheric circulation. *Journal of Geophysical Research: Atmospheres*, *124*(3), 1219-1232.

Bushell, A. C., Anstey, J. A., Butchart, N., Kawatani, Y., Osprey, S. M., Richter, J. H., ... & Yukimoto, S. (2020). Evaluation of the Quasi‐Biennial Oscillation in global climate models for the SPARC QBO‐initiative. *Quarterly Journal of the Royal Meteorological Society*.

Collimore, C. C., Martin, D. W., Hitchman, M. H., Huesmann, A., & Waliser, D. E. (2003). On the relationship between the QBO and tropical deep convection. *Journal of climate*, *16*(15), 2552-2568.

Elsbury, D., Peings, Y., & Magnusdottir, G. Variation in the Holton‐Tan effect by longitude. *Quarterly Journal of the Royal Meteorological Society*.

Garfinkel, C. I., & Hartmann, D. L. (2011). The influence of the quasi-biennial oscillation on the troposphere in winter in a hierarchy of models. Part I: Simplified dry GCMs. *Journal of the Atmospheric Sciences*, *68*(6), 1273-1289.

Garfinkel, C. I., Shaw, T. A., Hartmann, D. L., & Waugh, D. W. (2012). Does the Holton–Tan mechanism explain how the quasi-biennial oscillation modulates the Arctic polar vortex?. *Journal of the Atmospheric Sciences*, *69*(5), 1713-1733.

Gray, L. J., Anstey, J. A., Kawatani, Y., Lu, H., Osprey, S., & Schenzinger, V. (2018). Surface impacts of the quasi biennial oscillation. *Atmospheric Chemistry and Physics*, *18*(11), 8227-8247.

Hamilton, K., Hertzog, A., Vial, F., & Stenchikov, G. (2004). Longitudinal variation of the stratospheric quasi-biennial oscillation. *Journal of the atmospheric sciences*, *61*(4), 383-402.

Hansen, F., Matthes, K., & Gray, L. J. (2013). Sensitivity of stratospheric dynamics and chemistry to QBO nudging width in the chemistry–climate model WACCM. *Journal of Geophysical Research: Atmospheres*, *118*(18), 10-464.

Hersbach, H., Bell, B., Berrisford, P., Hirahara, S., Horányi, A., Muñoz‐Sabater, J., ... & Thépaut, J. N. (2020). The ERA5 global reanalysis. *Quarterly Journal of the Royal Meteorological Society*, *146*(730), 1999-2049.

411 Hitchman, M. H., & Huesmann, A. S. (2009). Seasonal influence of the quasi-biennial
412 oscillation on stratospheric jets and Rossby wave breaking. *Journal of the atmospheric*
413 *sciences*, *66*(4), 935-946.
414
415 Hitchman, M. H., Yoden, S., Haynes, P. H., Kumar, V., & Tegtmeier, S. (2021). An
416 Observational History of the Direct Influence of the Stratospheric Quasi-biennial
417 Oscillation on the Tropical and Subtropical Upper Troposphere and Lower Stratosphere.
418 *Journal of the Meteorological Society of Japan. Ser. II*.
419
420 Huang, B., Hu, Z. Z., Kinter, J. L., Wu, Z., & Kumar, A. (2012). Connection of
421 stratospheric QBO with global atmospheric general circulation and tropical SST. Part I:
422 Methodology and composite life cycle. *Climate dynamics*, *38*(1-2), 1-23.
423
424 Holton, J. R., & Tan, H. C. (1980). The influence of the equatorial quasi-biennial
425 oscillation on the global circulation at 50 mb. *Journal of Atmospheric Sciences*, *37*(10),
426 2200-2208.
427
428 Lu, H., Bracegirdle, T. J., Phillips, T., Bushell, A., & Gray, L. (2014). Mechanisms for the
429 Holton−Tan relationship and its decadal variation. *Journal of Geophysical Research:*
430 *Atmospheres*, *119*(6), 2811-2830.
431
432 Lu, H., Hitchman, M. H., Gray, L. J., Anstey, J. A., & Osprey, S. M. (2020). On the role
433 of Rossby wave breaking in the quasi−biennial modulation of the stratospheric polar

vortex during boreal winter. *Quarterly Journal of the Royal Meteorological Society*, *146*(729), 1939-1959.

Pahlavan, H. A., Fu, Q., Wallace, J. M., & Kiladis, G. N. (2021). Revisiting the quasi-biennial oscillation as seen in ERA5. Part I: Description and momentum budget. Journal of the Atmospheric Sciences, 78(3), 673-691.

Plumb, R. A., & Bell, R. C. (1982). A model of the quasi−biennial oscillation on an equatorial beta−plane. *Quarterly Journal of the Royal Meteorological Society*, *108*(456), 335-352.

Rao, J., Garfinkel, C. I., & White, I. P. (2020). Impact of the Quasi-Biennial Oscillation on the Northern Winter Stratospheric Polar Vortex in CMIP5/6 Models. *Journal of Climate*, *33*(11), 4787-4813.

Rao, J., Garfinkel, C. I., & White, I. P. (2020). How does the Quasi-Biennial Oscillation affect the boreal winter tropospheric circulation in CMIP5/6 models?. *Journal of Climate*, *33*(20), 8975-8996.

Richter, J. H., Anstey, J. A., Butchart, N., Kawatani, Y., Meehl, G. A., Osprey, S., & Simpson, I. R. (2020). Progress in simulating the quasi−biennial oscillation in CMIP models. *Journal of Geophysical Research: Atmospheres*, *125*(8), e2019JD032362.

457 Smith, K. L., Neely, R. R., Marsh, D. R., & Polvani, L. M. (2014). The specified
458 chemistry whole atmosphere community climate model (SC−WACCM). *Journal of*
459 *Advances in Modeling Earth Systems*, *6*(3), 883-901.
460
461 Son, S. W., Lim, Y., Yoo, C., Hendon, H. H., & Kim, J. (2017). Stratospheric control of
462 the Madden–Julian oscillation. *Journal of Climate*, *30*(6), 1909-1922.
463
464 Tegtmeier, S., Anstey, J., Davis, S., Ivanciu, I., Jia, Y., McPhee, D., & Pilch Kedzierski,
465 R. (2020). Zonal asymmetry of the QBO temperature signal in the tropical tropopause
466 region. *Geophysical Research Letters*, *47*(24), e2020GL089533.
467
468 Wang, C. C., & Magnusdottir, G. (2005). ITCZ breakdown in three-dimensional
469 flows. *Journal of the atmospheric sciences*, *62*(5), 1497-1512.
470
471 Wang, J., Kim, H. M., Chang, E. K., & Son, S. W. (2018). Modulation of the MJO and
472 North Pacific storm track relationship by the QBO. *Journal of Geophysical Research:*
473 *Atmospheres*, *123*(8), 3976-3992.
474
475 Yamashita, Y., Naoe, H., Inoue, M., & Takahashi, M. (2018). Response of the Southern
476 Hemisphere atmosphere to the stratospheric equatorial quasi-biennial oscillation (QBO)
477 from winter to early summer. *Journal of the Meteorological Society of Japan. Ser. II*.
478
479

480

481 **Figure 1**. Figure 1: DJ zonal mean zonal wind anomalies. Thin contours show
482 anomalies between +/- 8.5 m/s with intervals of +/- 1m/s. Thick contours correspond to
483 +10, 15, 20 … m/s. Gray shading denotes statistical significance, p-values < 0.05 via a
484 student's t-test, when comparing $QBO_{E50}$ anomalies to all other anomalies. To the right
485 of model titles is the number of DJ periods averaged together to make each composite
486 and the 10 hPa latitudinal width of the QBO. Widths are calculated by applying the "half-
487 maximum" method of Richter et al. (2020) and Bushell et al. (2020) to the anomalous 10
488 hPa response from each plot. Warm (cool) temperature anomalies are shown on FIg. 1q
489 with +/- 1 K contours.

490

491 **Figure 2:** ERA5 DJ 850 Kelvin PV anomalies. Anomalies are deviations from the
492 seasonal cycle for $QBO_{E50}$ indices. Hatching denotes statistical significance, p-values <
493 0.05 via a student' t-test, when comparing $QBO_{E50}$ anomalies to all other anomalies. The
494 contour interval in line and shading for all panels is +/- 10 PVU. Fifteen DJ seasons are
495 used to make the composite (a). Panel (b) shows the standard deviation of the field with
496 contour intervals 10, 20, 30… PVU.

497

498 **Figure 3:** Anomalies after imposing a $QBO_{E50}$ profile in the transient runs. (a-c): Zonal
499 mean meridional PV gradient for successive 30-day periods after branching: dashed-
500 negative (solid-positive) contours begin at negative (positive) $1x10^{-7}$ $K \cdot m \cdot kg^{-1} \cdot s^{-1}$ and
501 decrease (increase) by negative (positive) $5x10^{-7}$ $K \cdot m \cdot kg^{-1} \cdot s^{-1}$ intervals. The responses
502 at each isentrope are multiplied by $(/350)^{-9/2}$ to account for logarithmic change in PV with

503 height. (d-f): Latitude-time Hövmollers of 850 Kelvin PV (+/- 10 PVU) averaged over
504 0°E-120°E (d), 120°E-240°E (e), and (f) 240°E-360°E. Gray shading denotes statistical
505 significance in (a-f), p-values < 0.05 via a student's t-test, when comparing $QBO_{E50}$ and
506 control responses. (g-h) Maps of 850 K PV (+/- 10 PVU) anomalies with hatching
507 denoting statistical significance.
508
509 **Figure 4:** DJ 850 K PV anomalies for the 18 datasets. Contour intervals are +/- 10 m/s.
510 Hatching denotes statistical significance, p-values < 0.05 via a student's t-test, when
511 comparing $QBO_{E50}$ anomalies to all other anomalies. Black and blue rectangles denote
512 where the anomalous $_P$ is highly correlated with polar cap warming (Table S1).
513
514 **Figure 5:** Left: The anomalous meridional PV gradient ($_P$) over Asia is compared to the
515 anomalous 10 hPa polar cap (60°N+) temperature. $_P$ is not divided by the radius of
516 Earth when calculating it. Right: The anomalous 10 hPa QBO, longitudinally averaged
517 and cosine weighted latitudinally averaged zonal winds between 5°S-5°N, of Figure 1
518 are compared to $_P$ over Asia.